JOURNAL OF SOLID STATE CHEMISTRY 112, 429–437 (1994)

Structural Phase Transitions in the Ferromagnetic Vanadium Oxide NaV_6O_{11}

Yasushi Kanke,*[,1] Fujio Izumi,* Yukio Morii,† Etsuo Akiba,‡ Satoru Funahashi,† Katsuo Kato,* Mitsumasa Isobe,* Eiji Takayama-Muromachi,* and Yoshishige Uchida*

*National Institute for Research in Inorganic Materials, 1-1 Namiki, Tsukuba, Ibaraki 305, Japan; †Department of Materials Science and Engineering, Japan Atomic Energy Research Institute, Tokai, Naka, Ibaraki 319-11, Japan; and ‡National Institute of Materials and Chemical Research, 1-1 Higashi, Tsukuba, Ibaraki 305, Japan

Received December 27, 1993; in revised form June 3, 1994; accepted June 6, 1994

Neutron and X-ray diffraction experiments revealed that ferromagnetic NaV_6O_{11} (T_C = 64.2 K) undergoes two-step second-order structural phase transitions upon cooling: hexagonal ($P6_3/mmc$) → hexagonal ($P6_3mc$) → orthorhombic ($Cmc2_1$). Its structure at 200 K was determined by single-crystal X-ray analysis: hexagonal, $P6_3mc$, a = 5.7049(2) Å, c = 13.0796(8) Å, and Z = 2. The $P6_3/mmc \rightarrow P6_3mc$ transition is believed to accompany a magnetic transition at 245 K. V(1) octahedra, which construct an edge-sharing kagomé-type network, form a trimer on the $P6_3/mmc \rightarrow P6_3mc$ transition. V(2) octahedra, which form face-sharing dimers, separate into two nonequivalent types on the hexagonal–hexagonal transition. The $P6_3mc \rightarrow Cmc2_1$ transition occurs at a temperature between 35 and 40 K, which is lower than T_C. V(1) octahedra split into two nonequivalent types on the $P6_3mc \rightarrow Cmc2_1$ transition. The transitions are compared with those in V_2O_3, V_2O_4, and Li_xVO_2. The crystal structure of NaV_6O_{11} lacks the center of symmetry below T_C, which allows a canted-spin arrangement for the ferromagnetic state if the Dzyaloshinski–Moriya interaction exists. No structural phase transition was observed for SrV_6O_{11} (T_C = 70 K) between 22 and 373 K.

INTRODUCTION

V^{3+}–V^{4+} mixed-valence oxides are interesting in connection with the character of 3*d* electrons which are in a state intermediate between localized and itinerant ones. In contrast to the diversity of electric conductivity in vanadium oxides, neither ferromagnetic nor ferrimagnetic substance has been found except for AV_6O_{11} phases (A = Na, Sr) (1, 2), whose spontaneous magnetization is attributable exclusively to vanadium ions. These AV_6O_{11} phases are structurally related to magnetoplumbite-type compounds and crystallize in hexagonal $P6_3/mmc$ at room temperature (3). Resistivity perpendicular to [001], $\rho_\perp$, in NaV_6O_{11} shows normal metallic behavior below 80 K with a break point at 64.2 K corresponding to the Curie temperature (T_C) (1, 4). Above 80 K, $\rho_\perp$ decreases gradually and then increases above 245 K. Its magnetic susceptibility, χ, obeys the Curie–Weiss law above 245 K, and the χ^{-1} curve below 245 K is concave downward. Below 64.2 K, NaV_6O_{11} exhibits uniaxial magnetic anisotropy with the easy axis of magnetization parallel to [001].

SrV_6O_{11} shows magnetic phase transitions at 70 K ($=T_C$) and 320 K which correspond to those at 64.2 and 245 K in NaV_6O_{11}, respectively (2). In addition, SrV_6O_{11} shows metamagnetic behavior below 35 K. In contrast to NaV_6O_{11}, SrV_6O_{11} behaves as an insulator below T_C.

At room temperature (3), AV_6O_{11} phases have two octahedral V sites, V(1) and V(2), and a trigonal-bipyramidal site, V(3) (Fig. 1). The V(1) octahedra form an edge-sharing kagomé-type network perpendicular to [001]. Two V(2) octahedra adjoin each other across a mirror plane perpendicular to [001] and form a face-sharing dimer. The V(3) site is located on this mirror plane. Two adjacent coordination polyhedra of these V atoms share one corner if they are not equivalent.

In this paper, we will report two-step structural phase transitions in NaV_6O_{11} observed by both neutron and X-ray diffraction and discuss possible correlations between the structural and magnetic phase transitions. We will also discuss whether SrV_6O_{11} shows any structural phase transition.

EXPERIMENTAL

The single-crystal specimen of NaV_6O_{11} for X-ray diffraction was the same with that reported in Ref. (3). Its size was 0.20, 0.17, and 0.08 mm along [410], [2$\bar{3}$0], and [001], respectively. The NaV_6O_{11} powder for neutron diffraction was prepared by a solid-state reaction of $NaVO_3$, V_2O_3, and V_2O_5 at 993 K (4). The product contained a small amount of V_3O_5. NaV_6O_{11} for X-ray powder diffraction was obtained by crushing single crystals which were obtained from a mixture of $NaVO_3$ and V_2O_3 at a final

[1] To whom correspondence should be addressed.

0022-4596/94 $6.00

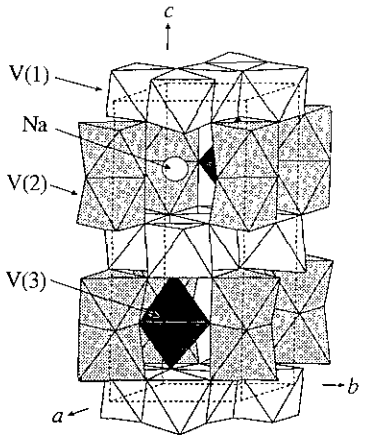

FIG. 1. Crystal structure of NaV_6O_{11} at room temperature. V(1) and V(2) atoms form VO_6 octahedra. The V(3) atom is located at the trigonal-bipyramidal site. The Na atom is coordinated to 12 O atoms.

heating temperature of 993 K (4). SrV_6O_{11} was prepared by heating a mixture of $Sr_2V_2O_7$ and V_2O_3 at 1473 K (5).

Single-crystal X-ray diffraction data of NaV_6O_{11} were collected at 200 K on an Enraf-Nonius CAD4 diffractometer with graphite-monochromatized Mo$K\alpha$ radiation (λ = 0.71073 Å) by ω–θ scan with $\Delta\omega = (0.8 + 0.35 \times \tan\theta)°$. The specimen was cooled by blowing cold N_2 gas. Lattice parameters were determined from the Bragg angles of 22 reflections in the region $82° < 2\theta < 90°$. Both hkl and $\bar{h}kl$ reflections for $0 \le h \le 9$, $0 \le k \le 5$, $0 \le l \le 26$, $|h| \ge |k|$ with $2\theta \le 90°$ were measured. Of the resulting 1258 reflections, 39 were unobserved, and 1217 satisfied the condition $I > 1.5\,\sigma(I)$. Standard reflections, 600, $\bar{4}80$, and 00$\underline{12}$, were measured every 4 hr. Because decreases in intensities were within 0.1% during the total exposure time of 102.1 hr, no decay correction was applied. Absorption-correction factors for F ranged from 1.336 to 1.758. Atomic scattering factors and anomalous dispersion terms for neutral atoms were taken from Ref. (6). Structural parameters were refined with SDP (7) by assigning anisotropic thermal parameters to all sites and applying extinction correction.[1]

Neutron-powder-diffraction data were collected on the HRPD diffractometer (8) installed at the JRR-3M reactor at JAERI. The incident neutron beam was monochromatized to give a wavelength of 1.823 Å using the 331 reflection of Ge. The sample was contained in a cylindrical vanadium cell. Except for a room-temperature measurement, the cell was placed in an aluminum chamber, and air in the chamber was replaced with He gas. The sample temperature was controlled by an He gas refrigerator.

X-ray powder-diffraction data were collected on a MAC Science MXP^3 diffractometer with Cu$K\alpha$ radiation and a curved graphite monochromator on the counter side. To minimize the preferred-orientation effect, the specimen was dispersed in an acetone solution of a cellulose resin, and the solid remaining after evaporation was ground to powder. It was mounted on a copper holder and cooled using an He gas refrigerator. The sample chamber was evacuated, and the sample holder was covered by an aluminum thermal-radiation shield. The sample holder was kept horizontal during the measurement.

RESULTS

The single-crystal data measured at 200 K show that NaV_6O_{11} has hexagonal symmetry and the reflection condition, $l = 2n$ for hhl. Possible space groups are therefore $P6_3/mmc$, $P\bar{6}2c$, and $P6_3mc$. $P6_3/mmc$ is centrosymmetric, but the other two are not. These three space groups were tested using the intensities of the 1217 reflections (Table 1). $P6_3mc$ gave the lowest R factors (models D and E). Both the R factors and the residual electron densities ($\Delta\rho$) for the model D were slightly lower than those for the model E. After collecting the data at 200 K, we also obtained intensity data at room temperature and confirmed that NaV_6O_{11} reverted to the $P6_3/mmc$ form. That is, NaV_6O_{11} undergoes a reversible phase transition $P6_3/mmc \rightleftarrows P6_3mc$ at a temperature between 200 K and room temperature. Prior to our work (3), NaV_6O_{11} was reported to crystallize in hexagonal $P\bar{6}2c$ at room temperature (9). However, the $P\bar{6}2c$ model for the room-temperature structure (9) is excluded if the hexagonal–hexagonal transition is of second or higher order. In the final refinement, the 1217 reflections were averaged into 1183 unique ones for $P6_3mc$ (R_{int} = 0.013). The model D afforded the results R = 2.2%, R_w = 3.9%, $w = 1/\sigma^2(F)$, $\Delta/\sigma < 0.005$, and $-2.18 \le \Delta\rho \le 2.04\ e\text{Å}^{-3}$. Table 2 lists the fractional coordinates and equivalent isotropic thermal parameters, and Table 3 gives the anisotropic thermal parameters. Throughout this paper, numbers in parentheses are estimated standard deviations in the last significant digits.

Neutron-powder-diffraction data for NaV_6O_{11} were collected at 30 and 106.5 K. The data indicate that $hh0$ reflections split into two peaks at 30 K, while $00l$ reflections do not (Fig. 2). Both the neutron and X-ray powder diffraction patterns at 30 K exhibit orthorhombic symmetry with relations $a_0 \approx a_h + b_h$, $b_0 = -a_h + b_h$, and $c_0 \approx c_h$. These patterns also show the reflection conditions, l =

[1] See NAPS document No. 05150 for 6 pages of supplementary material. Order from ASIS/NAPS, Microfiche Publications, P.O. Box 3513, Grand Central Station, New York, NY 10163. Remit in advance $4.00 for microfiche copy or for photocopy, $7.75 for up to 20 pages plus $.30 for each additional page. All orders must be prepaid. Institutions and organizations may order by purchase order. However, there is a billing and handling charge for this service of $15. Foreign orders add $4.50 for postage and handling, for the first 20 pages, and $1.00 for each additional 10 pages of material; add $1.50 for postage of any microfiche orders.

TABLE 1
Space-Group Examination on NaV_6O_{11} at 200 K Using the 1217 Reflections with $I > 1.5\ \sigma(I)$

Space Group	Model	N_p[a]	R (%)	R_w (%)	$\Delta\rho$ (e Å^{-3})
$P6_3/mmc$	A	24[b]	9.3	17.8	$-20.94 \le \Delta\rho \le +18.15$
$P\bar{6}2c$	B	24[c]	8.7	17.1	−22.13 +15.83
$P\bar{6}2c$	C[d]	24[c]	8.7	17.1	−22.10 +15.88
$P6_3mc$	D	43	2.3	4.0	−2.56 +2.05
$P6_3mc$	E[d]	43	2.3	4.1	−2.57 +2.06

[a] N_p is the number of structure parameters.
[b] Anisotropic thermal parameters cannot be assigned to O(2).
[c] Anisotropic thermal parameters can be assigned to neither O(1) nor O(2).
[d] Starting atomic coordinates for model C or E were derived from those of models B and D by changing (x, y, z) to $(x, y, -z)$ and $(-x, -y, z)$, respectively. The two models for each space group, B and C or D and E, are essentially congruent but differently related to the external form of the specimen.

TABLE 2
Fractional Coordinates and Equivalent Isotropic Thermal Parameters, B_{eq}, in NaV_6O_{11} at 200 K

Atom	Position	x	y	z	B_{eq} (Å^2)
V(1)	6c	0.49378(2)	$2x$	0	0.307(2)
V(21)	2a	0	0	0.14871(4)	0.298(5)
V(22)	2a	0	0	0.35341(4)	0.304(4)
V(3)	2b	1/3	2/3	0.74485(5)	0.305(3)
O(11)	6c	0.17102(15)	$2x$	0.08319(9)	0.60(1)
O(12)	6c	0.16969(11)	$2x$	0.42085(9)	0.24(1)
O(2)	6c	0.15282(11)	$2x$	0.74970(12)	0.65(1)
O(31)	2b	1/3	2/3	0.58907(16)	0.39(2)
O(32)	2b	1/3	2/3	0.90666(15)	0.23(2)
Na	2b	1/3	2/3	0.2549(2)	1.90(3)

Note. Hexagonal, $P6_3mc$, a = 5.7049(2) Å, c = 13.0796(8) Å, Z = 2, μ = 71.92 cm^{-1}, $F(000)$ = 474.0, R = 2.2%, R_w = 3.9%, $w = 1/\sigma^2(F)$, $\Delta/\sigma < 0.005$, and $-2.18 \le \Delta\rho \le 2.04$ e Å^{-3}. $B_{eq} = (8/9)\ \pi^2(4U_{11} + 4U_{22} + 3U_{33} - 4\ U_{12})$.

TABLE 3
Anisotropic Thermal Parameters in NaV_6O_{11} at 200 K

Atom	U_{11} (Å^2)	U_{22} (Å^2)	U_{33} (Å^2)	U_{12} (Å^2)	U_{13} (Å^2)	U_{23} (Å^2)
V(1)	0.00463(3)	U_{11}	0.00402(6)	0.00352(4)	0.00054(7)	$-U_{13}$
V(21)	0.00297(9)	U_{11}	0.0054(2)	$U_{11}/2$	0	0
V(22)	0.00423(9)	U_{11}	0.00310(13)	$U_{11}/2$	0	0
V(3)	0.00301(6)	U_{11}	0.00557(10)	$U_{11}/2$	0	0
O(11)	0.0086(2)	U_{11}	0.0061(3)	0.0047(3)	−0.0015(3)	$-U_{13}$
O(12)	0.00225(14)	U_{11}	0.0047(3)	0.0010(2)	0.0010(3)	$-U_{13}$
O(2)	0.0048(2)	U_{11}	0.0065(3)	−0.0040(4)	0.0024(4)	$-U_{13}$
O(31)	0.0058(4)	U_{11}	0.0034(5)	$U_{11}/2$	0	0
O(32)	0.0018(3)	U_{11}	0.0052(5)	$U_{11}/2$	0	0
Na	0.0163(4)	U_{11}	0.0395(12)	$U_{11}/2$	0	0

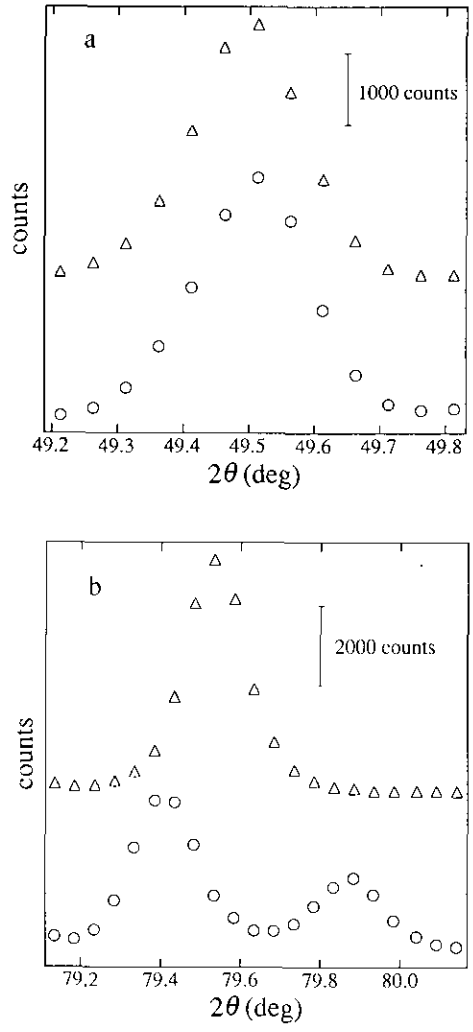

FIG. 2. Neutron-powder-diffraction patterns of NaV_6O_{11}. (a) shows 006_h reflections at 30 K (○) and 106.5 K (△). (b) shows 220_h reflections at 30 K (○) and 106.5 K (△).

TABLE 4
Structural Parameters of NaV_6O_{11} at 30 K

Atom	Position	x	y	z	B (Å^2)
V(1a)	4a	0	0.508(3)	0.003(4)	0.1
V(1b)	8b	0.265(3)	0.254(2)	0	0.1
V(21)	4a	0	−0.005(3)	0.147(3)	0.1
V(22)	4a	0	0.000(3)	0.351(3)	0.1
V(3)	4a	0	0.331(2)	0.241(3)	0.1
O(11a)	4a	0	0.826(4)	0.083(14)	0.10(4)
O(11b)	8b	0.249(5)	0.088(3)	0.080(14)	0.10
O(12a)	4a	0	0.830(5)	0.420(14)	0.10
O(12b)	8b	0.256(4)	0.084(4)	0.420(14)	0.10
O(2a)	4a	0	0.155(2)	0.256(14)	0.10
O(2b)	8b	0.230(2)	0.9278(12)	0.248(14)	0.10
O(31)	4a	0	0.336(4)	0.093(15)	0.10
O(32)	4a	0	0.334(5)	0.406(15)	0.10
Na	4a	0	0.659(3)	0.260(15)	0.4(5)

Note. Orthorhombic, $Cmc2_1$, and $Z = 4$. Neutron: $a = 5.6814(2)$ Å, $b = 9.9040(4)$ Å, $c = 13.0621(5)$ Å, $R_{wp} = 6.66\%$, $R_p = 5.20\%$, $R_I = 3.22\%$, $R_F = 5.06\%$, and $S = R_{wp}/R_e = 1.41$. X-ray: $a = 5.683(2)$ Å, $b = 9.903(4)$ Å, $c = 13.061(6)$ Å, $R_{wp} = 12.38\%$, $R_p = 9.71\%$, $R_I = 7.93\%$, $R_F = 3.54\%$, and $S = 2.40$. Parameters for the V atoms were refined using the X-ray data, and those for O and Na atoms using the neutron data. Isotropic thermal parameters, B, for all the V atoms were fixed at 0.1 Å^2, and those for all the O atoms were constrained to be equal.

$2n$ for $k = 0$ and $h + k = 2n$ for all reflections. Therefore, possible space groups are $Cmcm$, $C2cm$, and $Cmc2_1$, which are the maximal orthorhombic subgroups of $P6_3/mmc$, $P\bar{6}2c$, and $P6_3mc$, respectively (10).

Rietveld refinements of NaV_6O_{11} at 30 K were performed with RIETAN (11) using both the neutron and X-ray diffraction data. In neutron refinements, structural parameters of V atoms were fixed at those obtained by X-ray refinements. In the X-ray refinements, structural parameters of all atoms except for V were fixed at those obtained by the neutron refinements. The alternate refinements of the neutron and X-ray data were repeated until the structural parameters no longer varied appreciably. Though single-crystal data are required to test the possible three space groups, we adopted the $Cmc2_1$ model, assuming a second- or a higher order transition. The neutron data were analyzed by excluding diffraction peaks due to the aluminum chamber and regarding the sample as a mixture of NaV_6O_{11} and V_3O_5. Magnitudes of magnetic scattering from NaV_6O_{11} were examined by assuming a colinear magnetic-moment model with a spontaneous magnetization of 1.6 μ_B per formula unit. Because both observed and calculated intensities of magnetic scattering did not exceed the noise level, the magnetic scattering was neglected. Table 4 lists the crystal data of NaV_6O_{11} at 30 K, and Fig. 3 shows observed, calculated, and difference patterns.

X-ray powder-diffraction data show that the 220 reflection separates into two peaks below a temperature between 35 and 40 K (Fig. 4). Then, the $P6_3mc \rightarrow Cmc2_1$ transition occurs between 35 and 40 K, which is lower than T_C. That is, NaV_6O_{11} has two ferromagnetic forms with the $P6_3mc$ and $Cmc2_1$ space groups.

Neutron-powder-diffraction data for SrV_6O_{11} were collected at 22, 55, 100, 293, and 373 K (Fig. 5). In contrast to NaV_6O_{11}, no structural phase transition was observed for SrV_6O_{11} between 22 and 373 K. Lattice parameters a and c showed no significant shifts below 100 K, but increased with temperature above 100 K (Fig. 5). As in NaV_6O_{11}, intensities of reflections due to magnetic scattering were not strong enough to be detected.

DISCUSSION

$P6_3/mmc \rightarrow P6_3mc$ Transition in NaV_6O_{11}

On this transition, all the atoms in NaV_6O_{11} remain on $(1\bar{2}0)$ mirror planes, but its structure loses mirror planes perpendicular to [001] at $z = \frac{1}{4}$ and $\frac{3}{4}$. The V(2), O(1), and O(3) sites split into V(21) and V(22), O(11) and O(12), and O(31) and O(32), respectively (Table 2, Fig. 6). Table 5 shows interatomic distances and bond angles in NaV_6O_{11} at room temperature (3) and 200 K.

The V(1) octahedron is distorted in the $P6_3/mmc$ form (Table 5, Fig. 7). All of the O–V(1)–O bond angles are nearly 90°. However, the distance between the V(1) and apical O(3) atoms is longer than the distance between the V(1) and equatorial O(1) atoms. This distortion indicates that the d_ε state of the V(1) atom separates into two energy states, higher (d_{xy}) and lower (d_{xz} and d_{yz}) ones. Therefore, d electrons at the V(1) atom should occupy the degenerate band which consists of d_{xz} and d_{yz}. That is, the V(1) atom prefers the trivalent (d^2) state to the tetravalent (d^1) one. This idea is consistent with a Madelung-energy calculation (3), which suggests that the V(1) atom is trivalent.

In the $P6_3mc$ form, the V(1) octahedron shows not only the distortion described above but also an additional one (Table 5, Fig. 7). The V(1) atom deviates from the plane composed of the O(11) and O(12) atoms, to elongate the V(1)–O(31^{ii}) distance and shortens the opposite V(1)–O(32^{iii}) distance. The V(2) octahedron is highly distorted even in the $P6_3/mmc$ form (Table 5, Fig. 8). The O(2^{iv})–V(2)–O(2^{ix}) bond angle is acute, relaxing V(21)–V(22) Coulomb repulsion. The O(1)–V(2)–O(1^{viii}) bond angle is obtuse, which lets the O(1)–V(2)–O(2^{iv}) be nearly 90°. The V(21) and V(22) octahedra share a face; nevertheless the V(21)–O(2^{iv})–V(22) is acute, which suggests the existence of a V(21)–V(22) bond. The V(2) octahedron splits into two types on the transition, but its coordination situations remain almost unchanged between the $P6_3/mmc$ and $P6_3mc$ forms. The V(3) atom deviates from the regular triangle consisting of O(2)

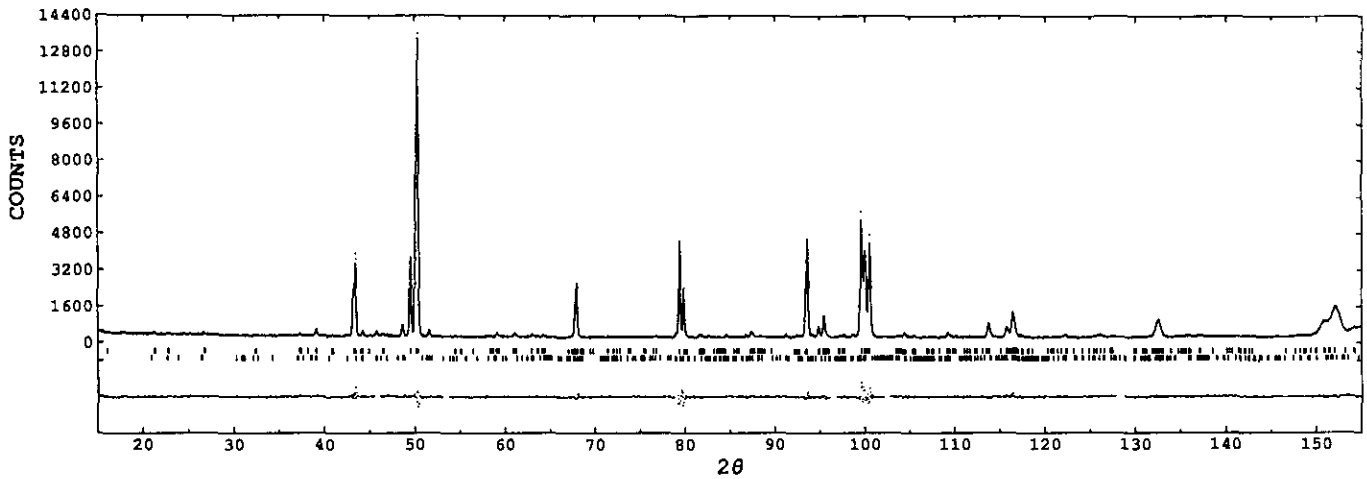

FIG. 3. Rietveld-refinement patterns obtained using the neutron data for NaV_6O_{11} at 30 K. The upper and lower tick marks indicate the Bragg angles of possible reflections for NaV_6O_{11} and V_3O_5, respectively.

atoms, which elongates the V(3)–O(32) distance and shortens the opposite V(1)–O(31) (Table 5).

The V(1)–V(1) distance exhibits the most remarkable change in interatomic distances on the transition. The V(1) atom shifts from the 6*g* position ($\frac{1}{2}$, 0, 0) in $P6_3/mmc$ and forms a V(1) trimer (Figs. 6 and 7). The V(1)–V(1) distance in the $P6_3mc$ form falls into two types: intertrimer and intratrimer (Table 5). In addition, all of the V(1)–O–V(1) bond angles change considerably on the transition while the other V–O–V angles do not.

NaV_6O_{11} shows anomaly in both resistivity and magnetic susceptibility at 245 K (1, 4). NaV_6O_{11} exhibits two ^{51}V NMR lines at 300 K (2). The lower frequency NMR line splits into two lines below 243 K, and their intensities are nearly equal to each other. The $P6_3/mmc \rightarrow P6_3mc$ transition is believed to accompany the magnetic transition at 245 K. Then the separation of the V(2) atom into different positions may cause the split of the NMR line at 243 K.

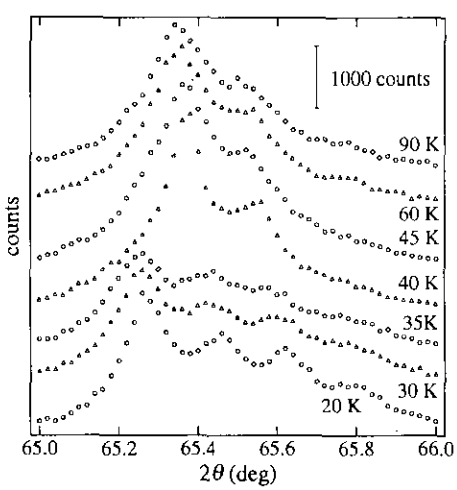

FIG. 4. Temperature dependence of the X-ray diffraction profiles for the 200 reflection in NaV_6O_{11}.

$P6_3mc \rightarrow Cmc2_1$ Transition in NaV_6O_{11}

All the atoms shift from the $(1\bar{2}0)$ planes of the hexagonal lattice on the transition. In the $Cmc2_1$ form, the V(1), O(11), O(12), and O(2) sites respectively split into V(1a) and V(1b), etc., owing to the loss of hexagonal symmetry (Table 4, Fig. 6).

NaV_6O_{11} shows a change in magnetization parallel to [001], $M_{//}$, at 50 K and that perpendicular to [001], $M_\perp$, at 35 K (1). Below 50 K, $M_{//}$ saturates and then increases linearly with increasing external magnetic field, H. Above 50 K, the linear relationship holds no longer. Below 35 K, $M_\perp$ is proportional to H up to 5.5 T. Above 35 K, $M_\perp$ begins to saturate at an H value less than 5.5 T. These results suggest that the spin structure in NaV_6O_{11} changes at 50 and/or 35 K. The change in $M_\perp$ at 35 K is supposed to accompany the $P6_3mc \rightarrow Cmc2_1$ transition which occurs between 35 and 40 K. The V(1) octahedra, which form the edge-sharing network perpendicular to [001], split into the two types in the $Cmc2_1$ form. The change in $M_\perp$ is therefore attributable to the split of the V(1) site.

Comparison with Phase Transitions in V_2O_3, V_2O_4, and Li_xVO_2

V_2O_3 has a corundum-type structure and undergoes a structural phase transition at 150–160 K upon cooling: rhombohedral $(R\bar{3}c) \rightarrow$ monoclinic $(I2/a)$ (12, 13), which accompanies a first-order metal-insulator transition (14, 15). This structural transition is a second-order transition

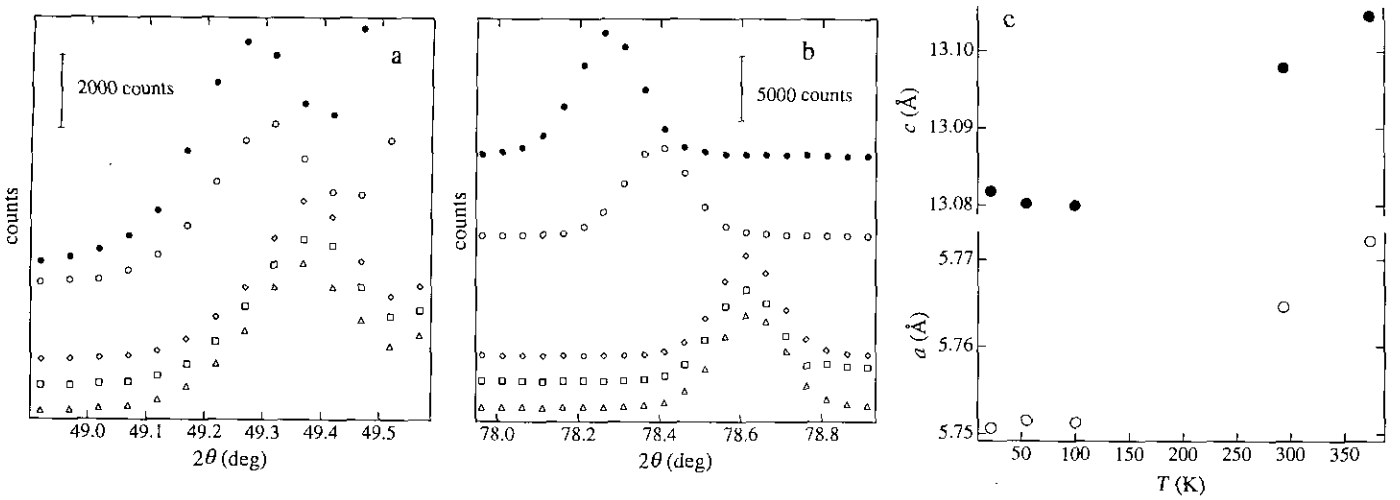

FIG. 5. Neutron-powder-diffraction profiles (a) and (b) and lattice parameters versus temperature (c) for SrV_6O_{11}. (a) and (b) respectively show 006 and 220 reflections at 22 K (△), 55 K (□), 100 K (◇), 293 K (○), and 373 K (●). The higher angle sides of 006 reflections are overlapped with strong 203 reflections (a).

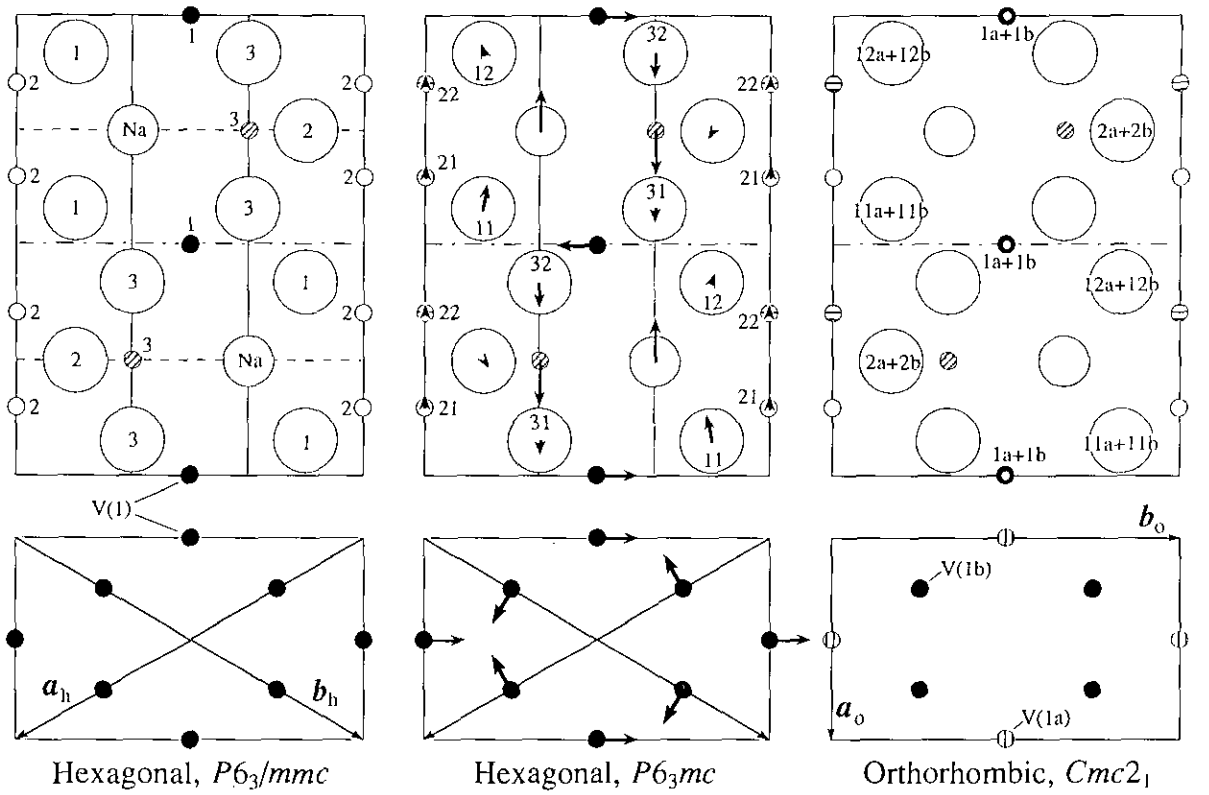

FIG. 6. Summary of the structural phase transitions in NaV_6O_{11}. The upper and lower figures respectively show (110) and (001) sectional views in hexagonal notation. Large, medium, and small circles indicate O, Na, and V atoms, respectively. Arrows in the middle figure indicate atomic displacements which are accompanied with the transition from the $P6_3/mmc$ form (room temperature) to the $P6_3mc$ form (200 K).

TABLE 5
Interatomic Distances (Å) and Bond Angles (°) in NaV_6O_{11} at Room Temperature (3), and 200 K (This Work)

	200 K ($P6_3mc$)	RT ($P6_3/mmc$)
V(1)–O(11^{i}) (×2)	1.9306(9)	1.9410(4)
O(12^{ii}) (×2)	1.9602(8)	
O(31^{ii}) (×1)	2.0677(11)	2.0327(6)
O(32^{iii}) (×1)	2.0010(12)	
V(21)–O(11) (×3)	1.8948(6)	1.9024(3)
O(2^{iv}) (×3)	2.0062(10)	2.0210(2)
V(22)–O(12) (×3)	1.8946(6)	1.9024(3)
O(2^{iv}) (×3)	2.0299(11)	2.0210(2)
V(3)–O(2) (×3)	1.78481(6)	1.7869(6)
O(31) (×1)	2.038(2)	2.086(1)
O(32) (×1)	2.117(2)	
Na–O(11) (×3)	2.760(3)	2.7436(5)
O(12) (×3)	2.707(3)	
O(2^{iv}) (×6)	2.8565(6)	2.8595(5)
V(1)–V(1^{v})	2.7460(1)	2.8562(1)
V(1^{vi})	2.9589(1)	
V(21)–V(22)	2.6773(7)	2.6840(4)
O(11^{i})–V(1)–O(11^{v})	92.02(3)	91.90(1)
O(12^{ii})–V(1)–O(12^{vii})	91.19(3)	
O(11^{i})–V(1)–O(12^{ii})	88.28(3)	88.10(1)
O(11^{i})–V(1)–O(31^{ii})	91.02(4)	92.02(2)
O(12^{ii})–V(1)–O(32^{iii})	92.38(4)	
O(11^{i})–V(1)–O(32^{iii})	91.28(4)	87.98(2)
O(12^{ii})–V(1)–O(31^{ii})	85.31(4)	
O(11)–V(21)–O(11^{viii})	101.13(4)	100.36(2)
O(11)–V(21)–O(2^{iv})	87.83(4)	88.58(2)
O(2^{iv})–V(21)–O(2^{ix})	81.36(4)	80.71(2)
O(12)–V(22)–O(12^{viii})	100.07(4)	100.36(2)
O(12)–V(22)–O(2^{iv})	88.97(4)	88.58(2)
O(2^{iv})–V(22)–O(2^{ix})	80.22(4)	80.71(2)
O(2)–V(3)–O(2^{i})	119.87(3)	120
O(2)–V(3)–O(31)	92.04(5)	90
O(2)–V(3)–O(32)	87.96(5)	
V(1)–O(11^{i})–V(1^{v}) (intratrimer)	90.66(4)	94.74(2)
V(1)–O(12^{ii})–V(1^{vi}) (intertrimer)	98.00(4)	
V(1)–O(32^{iii})–V(1^{v}) (intratrimer)	86.65(6)	89.27(4)
V(1)–O(31^{ii})–V(1^{vi}) (intertrimer)	91.37(7)	
V(21)–O(2^{iv})–V(22)	83.11(1)	83.22(1)
V(1)–O(11^{i})–V(21^{x})	129.03(4)	127.59(2)
V(1)–O(12^{ii})–V(22^{x})	126.18(3)	
V(1)–O(31^{ii})–V(3^{iv})	124.29(5)	125.78(3)
V(1)–O(32^{iii})–V(3^{iii})	127.60(4)	
V(21)–O(2^{iv})–V(3^{iv})	136.79(8)	138.39(1)
V(22)–O(2^{iv})–V(3^{iv})	140.10(8)	

Note. Symmetry codes: (i) $-x + y, 1 - x, z$; (ii) $y, 1 + x, -\frac{1}{2} + z$; (iii) $x, y, -1 + z$; (iv) $y, x, -\frac{1}{2} + z$; (v) $1 - y, 1 - x, z$; (vi) $-x + y, 2 - x, z$; (vii) $1 - x, 1 - x + y, -\frac{1}{2} + z$; (viii) $x, x - y, z$; (ix) $-x, y - x, -\frac{1}{2} + z$; (x) $x, 1 + y, z$.

like those in NaV_6O_{11}, because $I2/a$ is the maximal monoclinic subgroup of $R\bar{3}c$ (10). There are two types of V–V distances in the high-temperature $R\bar{3}c$ form of V_2O_3: across the shared oxygen octahedral face (2.700(1) Å) and across the shared octahedral edge (2.872(1) Å) (13). In the low-temperature $I2/a$ form, the former remains unique

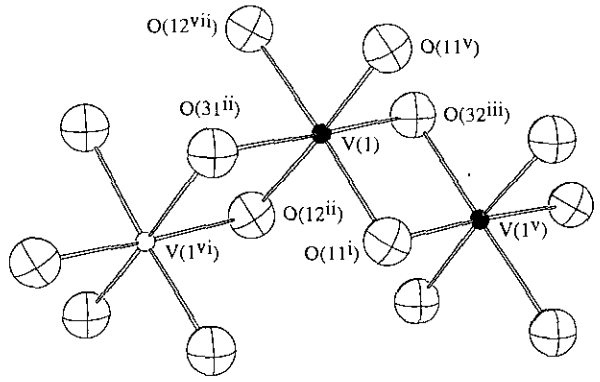

FIG. 7. Edge-sharing V(1) octahedra at 200 K drawn with ORTEP-II (31). Symmetry codes are listed in Table 5. The V(1) and V(1^{v}) atoms belong to the same V(1) trimer while the V(1^{vi}) atom belongs to another one.

(2.745(2) Å), but the latter corresponds to three different distances, 2.987(4), 2.861(9), and 2.876(9) Å with an average distance of 2.908 Å (13).

V_2O_4 has a rutile-type structure and shows a structural phase transition at ca. 340 K on cooling: tetragonal ($P4_2/mnm$) → monoclinic ($P2_1/c$) (16–18), which accompanies a first-order metal-insulator transition (14, 19). This structural transition is a first-order transition because $P2_1/c$ is not a maximal subgroup of $P4_2/mnm$ (10). If this transition occurred through an orthorhombic $Pnnm$ form, i.e., tetragonal ($P4_2/mnm$) → orthorhombic ($Pnnm$) → monoclinic ($P2_1/c$), both transitions should be of second order (10). The V–V distance in V_2O_4 is unique in the high-temperature $P4_2/mnm$ form: across the shared octahedral edge (2.869(6) Å) (18). It corresponds to two V–V dis-

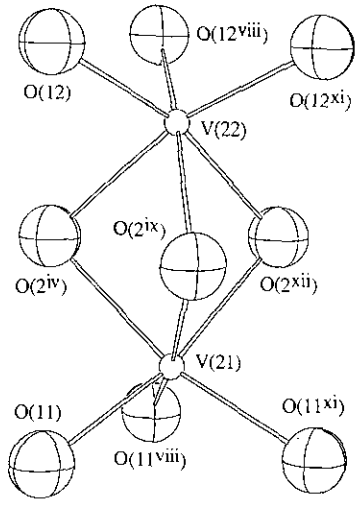

FIG. 8. Face-sharing V(21) and V(22) octahedra at 200 K drawn with ORTEP-II (31). Symmetry codes: (xi) $-y, -x, z$; (xii) $-x, -y, -\frac{1}{2} + z$. Remaining symmetry codes are listed in Table 5.

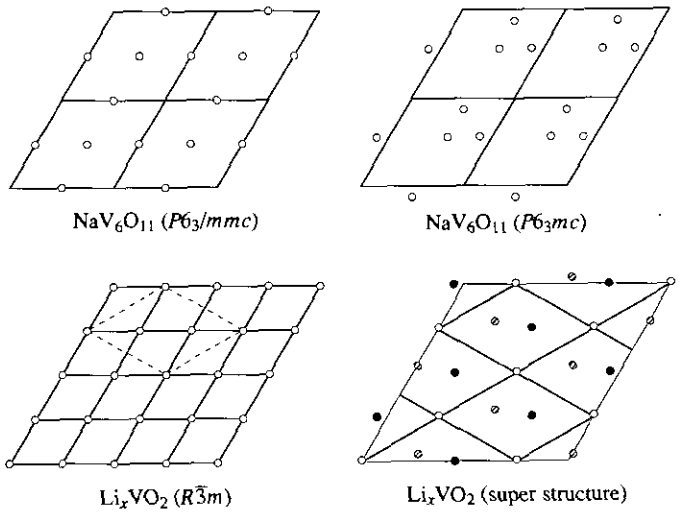

FIG. 9. Comparison of the V(1) network in NaV_6O_{11} (upper) with the V network in Li_xVO_2 (lower). The left figures show the high-temperature forms: $P6_3/mmc$ form (NaV_6O_{11}) and $R\bar{3}m$ form (Li_xVO_2). The right figures show the low-temperature forms: $P6_3mc$ form (NaV_6O_{11}) and superstructure form (Li_xVO_2). Circles and bold lines indicate V atoms and unit cells, respectively. The V atoms shown as open, closed, and hatched circles are not equivalent to each other.

tances in the low-temperature $P2_1/c$ form: 2.6191(4) and 3.1655(4) Å with an average distance of 2.8923 Å (17). Mean V–V distances in V_2O_3 and V_2O_4 increase on the transitions during cooling. However, mean V–V distances in NaV_6O_{11} decrease on the $P6_3/mmc \rightarrow P6_3mc$ transition (Table 5). This difference is consistent with the facts that V_2O_3 and V_2O_4 are insulators in their low-temperature forms and that the $P6_3mc$ form of NaV_6O_{11} is a conductor.

The metal-insulator transition in V_2O_3 has been explained in terms of the competition between the $3d$ bandwidth and electron correlation (20). The corresponding transition in V_2O_4 has been ascribed to a split in the d band which is caused by the pairing of V atoms owing to the structural phase transition (21). The low-temperature form of V_2O_3 shows antiferromagnetism (22). The corresponding form of V_2O_4 remains paramagnetic and exhibits no long-range magnetic order (23–25). On the other hand, NaV_6O_{11} and SrV_6O_{11} show spontaneous magnetization below T_C (1, 2).

At 573 K, Li_xVO_2 crystallizes in an ordered-rock-salt-type structure (rhombohedral, $R\bar{3}m$) (26). Its V octahedra form an edge-sharing network perpendicular to the hexagonal [001] direction. A quarter of the octahedral sites are vacant in the edge-sharing V(1) network of NaV_6O_{11}; consequently, the V(1) network forms a kagomé lattice. On the other hand, the corresponding octahedral sites are fully occupied in the V network of Li_xVO_2 (Fig. 9). The lattice parameters of Li_xVO_2 show discontinuity at ca. 460 K which corresponds to the first-order structural phase transition (27). The low-temperature form has a superstructure corresponding to $|a_{low}| \approx \sqrt{3} \times |a_{high}|$ and $|c_{low}| \approx 2 \times |c_{high}|$, with a reflection condition of $l = 3n$ for $00l$ (28). If the incommensurate structure along [001] (28) is disregarded, possible space groups for the low-temperature form are (i) trigonal $P3_1$, $P3_112$, $P3_121$, and their enantiomorphs, and (ii) hexagonal $P6_2$, $P6_222$, and their enantiomorphs. The four hexagonal space groups are ruled out because they do not allow the ordered-rock-salt structure. In every possible trigonal space group, the V site within the V network splits into three nonequivalent sites (Fig. 9), to give six independent V sites.

In the $P6_3mc$ form of NaV_6O_{11}, the V(1) atom occupies only one site with the V(1) trimer forming a regular triangle. In the low-temperature form of Li_xVO_2, on the other hand, the three V atoms which could form a "trimer" occupy nonequivalent positions so that the V atoms do not need to form the trimer (Fig. 9). If any, the shape of the trimer is not necessarily a regular triangle. Detailed structural studies are indispensable to obtain information about the electric and magnetic character of Li_xVO_2.

NaV_6O_{11} crystallizes in either $P6_3mc$ or $Cmc2_1$ below T_C, and both space groups lack the center of symmetry. Therefore, a canted-spin arrangement is allowed if the Dzyaloshinski–Moriya interaction (29, 30) exists. According to this theory (29, 30), each spin moment need not be colinear along [001] in both the $P6_3mc$ and the $Cmc2_1$ forms. Neutron-diffraction studies using single crystals are required to discuss the spin structures in NaV_6O_{11} and SrV_6O_{11} in detail.

CONCLUSION

NaV_6O_{11} (T_C = 64.2 K) shows two-step second-order structural phase transitions upon cooling: hexagonal ($P6_3/mmc$) → hexagonal ($P6_3mc$) → orthorhombic ($Cmc2_1$). The $P6_3mmc \rightarrow P6_3mc$ transition is believed to accompany a magnetic transition at 245 K. The $P6_3mc \rightarrow Cmc2_1$ transition occurs at 35–40 K, which is lower than T_C. In the $P6_3mc$ form, the V(1) atoms form the trimer, and the V(1)–V(1) distance across the shared octahedral edge falls into the longer intertrimer type and the shorter intratrimer type. In addition, the V(2) atoms separate into the two nonequivalent types. In the $Cmc2_1$ form, the V(1) atoms split into the two nonequivalent types. The transitions in NaV_6O_{11} are compared with those in V_2O_3, V_2O_4, and Li_xVO_2. The crystal structure of NaV_6O_{11} lacks the center of symmetry below T_C, which allows the canted-spin arrangement provided that the Dzyaloshinski–Moriya interaction exists. No structural phase transition was observed for SrV_6O_{11} between 22 and 373 K.

REFERENCES

1. Y. Uchida, Y. Kanke, E. Takayama-Muromachi, and K. Kato, *J. Phys. Soc. Jpn.* **60**, 2530 (1991).

2. Y. Uchida, Y. Kanke, and Y. Onoda, *in* "Proceedings 6th International Conference on Ferrites, Tokyo, 1992," p. 722.
3. Y. Kanke, K. Kato, E. Takayama-Muromachi, and M. Isobe, *Acta Crystallogr. Sect. C* **48,** 1376 (1992).
4. Y. Kanke, E. Takayama-Muromachi, K. Kato, and Y. Matsui, *J. Solid State Chem.* **89,** 130 (1990).
5. Y. Kanke, F. Izumi, E. Takayama-Muromachi, K. Kato, T. Kamiyama, and H. Asano, *J. Solid State Chem.* **92,** 261 (1991).
6. "International Tables for X-Ray Crystallography," Vol. IV. Kynoch Press, Birmingham, 1974.
7. B. A. Frenz and Associates, Inc., and Enraf–Nonius, "Structure Determination Package," 4th ed., 1985.
8. Y. Morii, K. Fuchizaki, S. Funahashi, N. Minakawa, Y. Shimojo, and A. Ishida, *in* Proceedings 4th International Symposium on Advanced Nuclear Research, Mito, 1992," p. 280.
9. M. E. de Roy, J. P. Besse, R. Chevalier, and M. Gasperin, *J. Solid State Chem.* **67,** 185 (1987).
10. "International Tables for Crystallography," Vol. A. Kluwer Academic, Dordrecht, 1992.
11. F. Izumi, "The Rietveld Method" (R. A. Young, Ed.), Chap. 13. Oxford Univ. Press, Oxford, 1993.
12. E. P. Warekois, *J. Appl. Phys.* **31,** 346S (1960).
13. P. D. Dernier and M. Marezio, *Phys. Rev. B* **2,** 3771 (1970).
14. F. J. Morin, *Phys. Rev. Lett.* **3,** 34 (1959).
15. H. Kuwamoto, J. M. Honig, and J. Appel, *Phys. Rev. B* **22,** 2626 (1980).
16. G. Andersson, *Acta Chem. Scand.* **10,** 623 (1956).
17. J. M. Longo and P. Kierkegaard, *Acta Chem. Scand.* **24,** 420 (1970).
18. S. Westman, *Acta Chem. Scand.* **15,** 217 (1961).
19. L. A. Ladd and W. Paul, *Solid State Commun.* **7,** 425 (1969).
20. N. F. Mott, *Rev. Mod. Phys.* **40,** 677 (1968).
21. J. B. Goodenough, *J. Solid State Chem.* **3,** 490 (1971).
22. R. M. Moon, *Phys. Rev. Lett.* **25,** 527 (1970).
23. T. Kawakubo and T. Nakagawa, *J. Phys. Soc. Jpn.* **19,** 517 (1964).
24. J. Umeda, H. Kusumoto, K. Narita, and E. Yamada, *J. Chem. Phys.* **42,** 1458 (1965).
25. K. Kosuge, *J. Phys. Soc. Jpn.* **22,** 551 (1967).
26. K. Imai, M. Koike, H. Sawa, and H. Takei, *J. Solid State Chem.* **102,** 277 (1993).
27. K. Kobayashi, K. Kosuge, and S. Kachi, *Mater. Res. Bull.* **4,** 95 (1969).
28. H. Takei, M. Koike, K. Imai, H. Sawa, H. Kadowaki, and Y. Iye, *Mater. Res. Bull.* **27,** 555 (1992).
29. I. Dzyaloshinski, *J. Phys. Chem. Solids* **4,** 241 (1958).
30. T. Moriya, *in* "Magnetism" (G. T. Rado and H. Suhl, Eds.), Vol. I, Chap. 3. Academic Press, New York, 1963.
31. C. K. Johnson, ORTEP-II, Report ORNL-5138. Oak Ridge National Laboratory, Tennessee, 1976.